HHS Public Access

Author manuscript

J Mol Med (Berl). Author manuscript; available in PMC 2019 November 01.

Published in final edited form as:

J Mol Med (Berl). 2018 November ; 96(11): 1227–1238. doi:10.1007/s00109-018-1694-x.

Ripor2 is involved in auditory hair cell stereociliary bundle structure and orientation

Oscar Diaz-Horta[#1], **Clemer Abad**[#1], **Filiz Basak Cengiz**[1], **Guney Bademci**[1], **Pat Blackwelder**[2,3], **Katherina Walz**[1], and **Mustafa Tekin**[1]

[1]Dr. John T. Macdonald Foundation Department of Human Genetics and John P. Hussman Institute for Human Genomics, University of Miami Miller School of Medicine, Miami, FL 33136, USA

[2]MGS/ RSMAS and UMCAM/Chemistry, University of Miami, Coral Gables, FL 33146, USA

[3]NSU Oceanographic Center, Dania Beach, FL 33004, USA

[#] These authors contributed equally to this work.

Abstract

RIPOR2 (previously known as FAM65B) localizes to stereocilia of auditory hair cells and causes deafness when its function is disturbed by mutations. Here we demonstrate that during the morphogenesis of the hair cell bundle, absence of Ripor2 affects the orientation of this key subcellular structure. We show that Ripor2 interacts with Myh9, a protein encoded by a known deafness gene. Absence of Ripor2 is associated with low Myh9 abundance in the mouse cochlea despite increased amount of *Myh9* transcripts. While Myh9 is mainly expressed in stereocilia, a phosphorylated form of Myh9 is particularly enriched in the kinocilium. In *Ripor2* deficient mice, kinocilium shows an aberrant localization which associates with a reduced content of phosphorylated Myh9. Acetylated alpha tubulin, another specific kinociliary protein which contributes to microtubule stabilization, is reduced in the absence of Ripor2 as well. We propose that Ripor2 deficiency influences abundance and/or post-translational modifications of proteins expressed in both stereocilia and kinocilia. This effect may have a negative impact on the structure and function of the auditory hair cell bundle.

Keywords

Deafness; Hair cells; Kinocilium; Myh9; Ripor2; Stereocilia

INTRODUCTION

Hair cells in the mammalian cochlea are specialized mechanosensory receptors that convert sound-induced vibrations into electrochemical signals. In mice, as early as E14, the apical portion of auditory hair cells shows two types of protrusions: a single true or microtubule-based cilium called kinocilium, and several actin-based microvilli [1]. During development,

Corresponding Authors: Katherina Walz, Ph.D., kwalz@med.miami.edu, Mustafa Tekin, MD, mtekin@med.miami.edu.

Conflict of Interest Statement. None declared

some microvilli eventually become stereocilia - structures that resemble hair-like projection- by remodeling their actin-core and the kinocilium migrates to the lateral side of the cell positioning at the vertex of the developing stereociliary bundle [1]. The hair cell bundle adopts a shape consisting of stereocilia lined up in several rows of increasing height, similar to a staircase. Planar cell polarity (PCP) pathway and other intrinsic polarity pathways are likely to underlie morphological and molecular asymmetry across the bundle. The kinocilium has been proposed to modulate cell polarity because the migration of this structure predicts the orientation of the mature stereociliary bundle [2]. The kinocilium degenerates postnatally and its role in directing polarization is merely developmental. Stereocilia at its core is composed of parallel actin filaments highly crosslinked [3]. The paracrystal core is stiff but hinges at the base where the protrusion tapers. Stereocilia shape and properties are the result of intrinsic and extrinsic factors that modulate the structure and dynamics of the actin core. These factors include proteins that influence the rate of actin polymerization and de-polymerization, actin cross-linkers, myosins and their binding partners [1]. The mechanotransduction channel in which the auditory perception originates is located in stereocilia but its molecular composition still remains poorly characterized [4].

We have recently identified RIPOR2 (previously known as FAM65B) as an essential protein required for normal hearing in humans [5]. The initial characterization using confocal microscopy in the murine organ of Corti showed that the protein localizes to the apical membrane of hair cells and stereocilia [5]. A more recent study shows that a Ripor2 deficient mouse model is profoundly deaf with impaired mechanotransduction [6]. High resolution STORM microscopy has shown that Ripor2 localizes to the taper of the stereocilia forming ring-like oligomeric structures [6]. Scanning electron microscopy (SEM) indicates that in the absence of Ripor2, stereocilia show abnormally shaped basal domains and from the apical hair cell surfaces emerge abnormal protrusions [6]. On the other hand, it remains unclear how such particular subcellular localization of Ripor2 is related to other findings in this animal model, including the mislocalization of the kinocilium and the abnormal hair bundle orientation and arrangement [6].

Ripor2 has been reported to interact with several proteins including the small GTPases RhoA and RhoC, a histone deacetylase Hdac6, and the skeletal muscle protein dysferlin [7]. In auditory hair cells, homophilic interactions between Ripor2 molecules require RhoC [6], a previously documented protein partner [8]. In the present study, we investigate interacting partners of Ripor2 within the auditory hair cells. We show that Ripor2 interacts with Myh9, a protein previously implicated in deafness [9]. We further reveal that Ripor2 regulates the abundance and post translational modifications (PTM) of proteins highly expressed within the kinocilium suggesting a critical role in hair bundle morphogenesis.

MATERIALS AND METHODS

Animal use and Generation of *Ripor2* KO mice

All procedures were approved by the University of Miami Institutional Animal Care and Use Committee and followed the National Institutes of Health guidelines “Using Animals in Intramural Research (http://oacu.od.nih.gov/training/PI/main_menu.htm).”)

The *Ripor2*$^{tm1(KOMP)Vlcg}$ mouse strain used for this research project was created from embryonic stem (ES) cell clone 15686A-B6, generated by Regeneron Pharmaceuticals, Inc. and made into live mice by the KOMP Repository (www.komp.org) and the Mouse Biology Program (www.mousebiology.org) at the University of California Davis. The ES cells possessed an allele [*Ripor2*$^{tm1(KOMP)Vlcg}$] with an ablating deletion of the Ripor2 gene, which was replaced by the *lacZ* gene (VelociGene KOMP definitive null allele design, *ZEN-Ub1* cassette)[10]. The ES cells were injected into C57BL/6 mouse blastocysts, and chimeric mice in a complete C57BL/6 genetic background were generated. Male chimeric mice were selected by VelociGene KOMP allele PCR genotyping strategies by using primers NeoFwd and SD and mated with normal female C57BL/6 mice to generate C57BL/6 mice with a heterozygous genotype of the *Ripor2* gene (*Ripor2*$^{+/-}$). *Ripor2* KO mice with a homozygous genotype (*Ripor2*$^{-/-}$) were obtained by crossing male and female *Ripor2*$^{+/-}$ C57BL/6 mice.

Ripor2 mRNA expression

Expression of Ripor2 mRNA of wild type of mutant mice was assessed by RT-PCR. Reactions were performed using primers: mRipor2_exp_f, mRipor2_exp_r, mGapdh_Exp_f, mGapdh_Exp_r (Supplementary Table S1).

Mouse phenotypic characterization

General characteristics and reflexes—Mice were evaluated for general health which included body weight, observation of coat and fur condition, visual placing and reflexive reactions to a cotton swab gently touching whiskers, and finally observation of vocalization during handling and circling behavior.

Rotarod—Mice were place on an accelerating rotarod apparatus for three trials with a 15 minute rest interval between trials. Each trial lasted for a maximum of 600 s, during which the rod accelerated linearly from 4 to 40 rpm. The amount of time for each mouse to fall from the rod was recorded for each of the trials.

ABRs and DPOAEs—To assess hearing capabilities, auditory brainstem responses (ABRs) and distortion product optoacoustic emissions (DPOAEs) were recorded and analyzed. Prior to testing, animals were anesthetized intraperitoneally using a mixture of ketamine (100 mg/kg) and xylazine (20mg/kg). One dosage of this mixture allowed for animals to remain anesthetized for the entirety of the test. Using a heating pad, the body temperature of the mice was kept at 37 °C for the duration of the test and the recovery period. DPOAEs were measured and recorded first followed by the ABRs. Both tests were conducted using a Smart EP Universal Smart Box (Intelligent Hearing Systems, Miami, FL).

X-gal staining

Inner ears were dissected from mice in PBS 1X and fixed for 30 min on ice in 4% paraformaldehyde. Free floating inner ears were incubated overnight in X-gal staining solution (0.02% NP40, 0.01% sodium deoxycholate, 2mM $MgCl_2$, 5mM $K_3Fe(CN)_6$, 5mM $K_4Fe(CN)_6$, 0.5 mg/ml X-gal in PBS 1X), washed twice in PBS 1X and fixed a second time in 4% PFA for 90 min.

Generation of expression constructs

Wild type *RIPOR2* cDNA was synthesized from control blood RNA using SuperScript III (Invitrogen) and random hexamers (Promega). Full-length wild type *RIPOR2* lacking the stop codon was amplified by high-fidelity PCR using Long Expand Taq Polymerase (Roche) and a primer pair (RIPOR2-TOPO-F, RIPOR2-TOPO-R, Table S1). The resulting amplicon was cloned into a pcDNA3.1/CT-GFP-TOPO vector (Invitrogen) [5]. To substitute the c-terminus GFP Tag for a HA tag, primers EcoRV_HA_NotI_F and EcoRV_HA_NotI_R were annealed to form double-stranded DNA. Both, the double strand fragment containing the HA ORF and the plasmid containing RIPOR2-GFP were digested with EcoRV and NotI and ligated. The resulting plasmid containing RIPOR2-HA was Sanger sequenced. MYH9-Myc cloned into the expression vector pEZ-M09 was obtained from Genecopoeia.

Transfection, Immunoprecipitation, Co-immunoprecipitation and Western Blot

Seventy percent confluent HEK293 cell monolayers cultured on a 10 cm^2 dishes were transfected with the RIPOR2-HA construct using Lipofectamine 3000 (Invitrogen) following the manufacturer's standard instructions. Forty-eight hours post-transfection cells were washed with PBS and proteins were extracted with cold lysis buffer (Pierce) containing a protein inhibitor mixture (Sigma). Dissected cochleae from wild type mice were also subject to protein extraction using the same buffer and inhibitors. Protein concentration was measured using the BCA Protein Assay kit (Pierce). Immunoprecipitations were performed with anti-HA and anti-c-Myc coupled magnetic beads (Pierce) to avoid having immunoglobulins in the protein eluates. In brief, 500 μg of total cell lysates or cell/cochlear tissue combined lysates were incubated with either specific anti-HA antibody coupled magnetic beads (Thermo Scientific) or anti-c-Myc antibody coupled magnetic beads (Thermo Scientific) as control, at 4°C overnight. Beads were washed twice with the manufacturer's immunoprecipitation lysis and wash buffer. Samples were boiled with a lane marker containing reducing agent at 100°C for 5 min. Protein samples were run in SDS-PAGE gels and silver stained using the Silver Stain for Mass Spectrometry kit (Pierce). Bands that were present in protein extracts pulled down with the anti-HA beads in the presence or absence of wildtype mouse protein extracts obtained from dissected cochleae but absent in the HEK293 protein extracts precipitated with anti-c-Myc beads were excised and sent to the Scripps Center for Metabolomics and Mass Spectrometry for protein identification. For co-immunoprecipitation experiments, cells were transfected as described above but with either RIPOR2-HA/MYH9-Myc or MYH9-Myc constructs. Pulldowns were performed with the Crosslink Magnetic IP/Co-IP Kit (Pierce) according to the manufacturer's instructions. 500 μg of total cell lysates were incubated with 5 μg of either a mouse anti-HA antibody (Abcam) or control mouse immunoglobulin G (Santa Cruz) at 4°C overnight. The lysate-antibody mixtures were incubated with protein A/G magnetic beads (Thermo Scientific) at room temperature for 1 hr on a rotator mixer. Beads were collected with a magnetic stand. Beads were washed twice with the manufacturer's immunoprecipitation lysis and wash buffer. Samples were boiled with a lane marker containing reducing agent at 100°C for 5 min. For western blots pulldown samples were loaded onto precast 4–20% gradient SDS-polyacrylamide gels (Lonza) and transferred to a 0.2-μm PVDF membrane (Bio-Rad). Immunodetection was performed using anti-HA (Abcam) and anti-Myc (Cell Signaling) as primary mouse antibodies. The secondary

antibody consisted on an anti-mouse-HRP conjugated antibody (Cell Signaling). The results were visualized by chemiluminescence using Pierce ECL Western Blotting Substrate (Thermo Scientific). For western blots assessing abundance of endogenous cochlear proteins we followed the protocol as previously described but using the appropriate primary antibodies as corresponded. Primary antibodies utilized are anti-acetylated-α-tubulin mouse monoclonal antibody (T7451, Sigma-Aldrich), anti-Ripor2 rabbit polyclonal antibody (HPA031245, Sigma), anti-Myh9 mouse monoclonal antibody (H00004627M01, Abnova), anti-Myh9-phospho-S1943 rabbit polyclonal antibody (ab2974, EMD Millipore), anti-β-tubulin rabbit polyclonal antibody (ab15708, EMD Millipore) and anti-Gapdh mouse monoclonal antibody (sc-47724, Santa Cruz Biotechnology).

Immunocytochemistry

To investigate the interaction of RIPOR2 and MYH9 in cells expressing both proteins, 70% confluent and COS-7 cells grown on coverslips placed in six well plates were transfected. RIPOR2-HA and MYH9-Myc constructs were used as transfection vectors. Lipofectamine 3000 (Invitrogen) was the transfection agent utilized following the manufacturer's standard instructions. Forty-eight hours post transfection, cells were washed with PBS and fixed with 4% PFA/PBS solution. Cells were permeabilized with 0.5% Triton/PBS for 20 min, blocked with 5% BSA, and then an anti-HA-Tag rabbit monoclonal antibody (Cell Signaling) and a mouse anti-Myc-Tag (Cell Signaling) were applied for 1 h. Specimens were washed with PBS, and antirabbit Alexa Fluor 488, and anti-mouse Alexa Fluor 568 were applied. Phalloidin-Alexa Fluor 647 (Life Technologies) and DAPI (Calbiochem) were used to counterstain for actin and nuclear DNA, respectively. Specimens were washed with PBS and mounted in fluorescence mounting medium (Dako). Preparations were imaged using 63× objectives with a Zeiss LSM 710 fluorescence microscope.

For Whole-Mount immunofluorescence of organ of Corti, P4 mice cochlea neuroepithelia were microdissected and fixed in 3% paraformaldehyde (PFA), permeabilized in 0.5% Triton X100, and incubated overnight in blocking solution [5% (wt/vol) BSA in PBS]. Specimens were incubated with primary antibodies at room temperature for 2 hours. After three PBS 1× washes, samples were incubated with species specific fluorescent secondary antibodies for 1 h. The specific counter staining reagents were also used as corresponded. Inner ear neuroepithelia were mounted in ProLong Gold Antifade Reagent (Invitrogen) and imaged with a 63× objective with a Zeiss LSM 710 fluorescence microscope.

For quantification of hair cell planar polarity we followed a previously described protocol [11]. Briefly, the organ of Corti was imaged by confocal microscopy at three positions corresponding to 25%, 50% and 75% of the length of the cochlea measured from the base. The orientation of individual hair cells (inner hair cells and the three rows of outer hair cells) was measured using the ImageJ (NIH) angle measurement tool. The short arm of each angle was drawn from the α-acetylated tubulin labeled kinocilium and across the center of the hair cell. The long arm of each angle was drawn parallel to three adjacent hair cells within the same row. Measurements of individual hair cell bundle orientation angles were assembled using Oriana 4 circular graphing software (Kovach Computing Services). These analyses

were completed for each genotype at the three cochlear positions. Statistical significance was calculated by $\chi 2$ test using Oriana 4.

Scanning Electron Microscopy

Cochleae were dissected and placed in 2% gluteraldehyde in PBS. Samples were rinsed in three changes of PBS for 5 mins each. Cochleae were then post-fixed in .01M osmium tetroxide in PBS for 2 hour, and rinsed 3 times in PBS for 5 mins each. Samples were dehydrated in a graded series of ethanol to 100% and dried in hexamethyldisilazane. After outgassing overnight, samples were coated with Pd in a sputter coater and imaged using an XL-30 field emission scanning electron microscope.

RESULTS

Ripor2 knockout mice are profoundly deaf with conserved vestibular function

The *Ripor2* knockout (KO) mouse carried a deletion of exons 2 to 14 in the *Ripor2* gene (Fig. S1A). The longest transcript of *Ripor2* (NM_029679.2) contains 23 exons. Mice were generated in a complete C57BL/6 genetic background [10]. The presence of *Ripor2* transcripts was tested by RT-PCR using primers designed to amplify a fragment of *Ripor2* comprising exons 3 and 7 (mRipor2_exp_f and -r, Table S1). The amplification product was absent in $Ripor2^{-/-}$ mice (Fig. S1B). General characteristics were examined and no significant difference was observed in coat condition, presence of barbering, piloerection, presence of whiskers, and body weight between $Ripor2^{-/-}$ mice and the controls littermates. Visual placing reflex and reactions to a gentle cotton swab touch to the whiskers were also normal. A lower vocalization frequency was observed when handling $Ripor2^{-/-}$ mice (n=6) as compared with wild type littermates (n=6) (* $p < .001$ chi-square test) (Fig. S1C). Absence of circling and balance defects as well as a normal performance in the rotating rod tests suggest a normal vestibular function for *Ripor2* KO mouse (Fig. S1D). Auditory brain-stem responses (ABRs) assesses the function of the cochlea along its entire spiral dimension. ABRs were recorded upon delivering sound stimuli with varying frequencies (click and 8–24 kHz) and intensities (20–100 dB) in both WT and *Ripor2* KO mice. In *Ripor2* KO mice, average ABR thresholds for the click and all tested frequencies (pure tones) were >90 dB, indicating profound hearing loss (Fig. 1A). We also measured distortion product evoked otoacustic emissions (DPOAEs) to assess the amplification of cochlear vibration provided by electromotility of outer hair cells (OHCs). DPOAEs amplitudes produced by *Ripor2* KOs were reduced in all the tested frequencies (Fig. S1E).

To determine the spatiotemporal expression of *Ripor2* in the inner ear of heterozygous *Ripor2* LacZ/+ we used X-gal staining taking advantage of the LacZ insertion within the *Ripor2* gene. Whole inner ears were stained at three developmental stages: $E_{15.5}$, $E_{19.5}$ and P_0 (Fig. 1B). In cochlea, *Ripor2* was undetected at $E_{15.5}$, while highest X-gal signals were observed in $E_{19.5}$ and decreased by P_0. Strongest signals were found in inner and outer hair cells as well as in Hensen's cells. Expression of *Ripor2* was detected in utricle and ampulla in all three studied stages in increasing manner (Fig. 1B). To evaluate the effect of Ripor2 deficiency in hair cell morphology along the extension of the cochlear sensory epithelium, cochlear whole mounts were obtained from wild type and *Ripor2* KO mice at P_4 and stained

with phalloidin, a selective toxin that tightly binds f-actin. Both types, outer and inner hair cell stereociliary bundles of *Ripor2* deficient mice show orientation defects in all three regions of the cochlea: the base, middle and apex (Fig. 1C). Higher resolution scanning electron microscopy (SEM) images show also defective stereocilia interconnection, organization and orientation in both hair cells types from *Ripor2* KO mice (Fig. 1D). To determine at which developmental stage the absence of Ripor2 affects cochlear PCP, quantification of the hair cell bundle orientation was performed in wild type and *Ripor2* KO mice at $E_{18.5}$ and P_5. By $E_{18.5}$, the kinocilium reaches the lateral position along the mediolateral axis and stereociliary bundles are regularly organized [12, 13]. Postnatally, the stereociliary bundle completes its maturation and the kinocilium regresses until it disappears at P_{21}[14]. Using an alpha-acetyl tubulin antibody as a specific kinocilium marker, we show that the typical position of the kinocilium and the orientation of the hair bundle are impaired in *Ripor2* KO mice (Fig. 2A). Deviations (>5 °) from the mediolateral axis were more frequent in stereociliary bundles from inner and outer hair cells of *Ripor2* KO mice when compared to wild type animals (Fig. 2B). These differences were found in both developmental time points.

RIPOR2 interacts with Myh9

Most RIPOR2 interaction partners have been found using yeast-two-hybrid technology (i.e. GTPases RhoA and RhoC) [6, 8] and immunoprecipitation methods (i.e. Hdac6, dysferlin, myoferlin) in myoblasts [7]. Considering that each cell type expresses a distinctive proteome, and that many of protein-protein interactions are reversible [15], we combined protein extracts from HA-tagged RIPOR2 overexpressing HEK293 cells with protein extracts from wild type mouse cochlea. Immunoprecipitation of the combined protein extract with an anti-HA antibody coupled beads was followed by PAGE electrophoresis and silver staining. Mass spectrometry (MS) analysis of the excised band (indicated with an asterisk) revealed the presence of Myh9 (Fig. 3A). Note that Myh9 is exclusively present in the combined cell and cochlear extracts immunoprecipitated with anti-HA antibody coupled beads. The RIPOR2-MYH9 interaction was validated by co-immunoprecipitation using HEK293 cells overexpressing both proteins with two different tags (Fig. 3B) and by immunohistochemistry (Fig. 3C).

To further assess the interaction of Ripor2 and Myh9 in the auditory epithelium, we analyzed the expression of both proteins by immunohistochemistry in cochlear whole mounts. Myh9 (red signals) shows an expression pattern similar to actin staining (blue signals) which is consistent with a stereociliary localization (Fig. 4A). We validated the specificity of the antiMyh9 antibody by transfecting COS-7 cells with a mammalian expression vector encoding for HA-tagged MYH9. Signals corresponding to anti-Myh9 and to anti-HA antibodies show overlapping recognition patterns (Fig. S2).

We also confirmed the previously reported localization of Ripor2 (green signals) to the basal end of the stereocilia near the taper region [6] in both, outer and inner hair cells (Fig. 4A). It is intriguing that some signal corresponding to Ripor2 is also visible in the surface of Deiters' cells, especially because only hair cells and Hensen's cells show positive x-gal

staining (Fig. 1B) [6]. Lastly, co-staining of hair cells with antibodies recognizing both Ripor2 and Myh9 shows co-localization near the taper of stereocilia (Fig. 4F).

Lack of Ripor2 associates with decreased abundance of Myh9

Immunohistochemistry of whole mounts of cochlea at P4 shows that expression of Myh9 in hair cells from *Ripor2* deficient mice was considerably reduced (Fig. 4B) compared to wild type animals (Fig. 4A). Western blot analysis using specific antibodies shows that cochlear protein extracts from *Ripor2* deficient mice contain less amount of total Myh9 (Fig. 4C, D). qPCR analysis shows an increased number of *Myh9* amplicons in KO mice cochlea (Fig. 4E).

S1943 Phosphorylated Myh9 is located in the hair cell kinocilium

Non-muscle myosins II (NM II) are subject to post-translational modifications that regulate their structure and function [16]. S-1943 phosphorylation at the non-helical tail piece of NM IIA heavy chain (encoded by *MYH9*) regulates filament assembly and subcellular localization [17]. Interestingly, an anti-phospho-S1943-MYH9 antibody show expression in the hair cell kinocilium of inner and outer hair cells as well as in the cilium of supporting cells (Fig. 5A). Simultaneous staining of both phospho-Myh9 and alpha-acetyl tubulin shows that they colocalize along the length of the kinocilium except in the base in which pure signals corresponding to phospho-Myh9 (green) are clearly distinguishable (Fig. 5B, left panel). In KO animals, phospho-Myh9 signals are weak and do not show discernible presence in the base as for WT kinocilium. In addition, western blot analysis indicates that abundance of phospho-Myh9 is also reduced in KO mice cochlea (Fig. 5C,D).

Considering the previously reported inhibitory effect of Ripor2 on HDAC6 enzymatic activity [7], we also evaluated if Ripor2 may influence PTMs of α-tubulin. Western blot analysis shows a decrease on the content of alpha-acetyl-tubulin in protein extracts from cochleae of Ripor2 deficient mice (Fig. 5E, F).

DISCUSSION

Ripor2 has two paralog genes showing 70% of sequence similarity: *Ripor1 (Fam65a) and Ripor3 (Fam65c),* Rho family-interacting cell polarization regulator 1 and 3, respectively. Although impairment of *Ripor2* leads to non-syndromic deafness in humans [5] and mice [6], *Ripor2* is expressed in many tissue types of mouse [6] (Fig. S1B). Compensatory mechanisms including genetic redundancy may play a role in the non-syndromic nature of *Ripor2* mutations. Likewise, *Ripor2* KO mouse shows a normal vestibular function (Fig. S1C and D) despite the fact that *Ripor2* expression starts earlier in vestibular than in cochlear compartments during the inner ear development (Fig. 1B).

RIPOR2 has been shown to express at the apical plasma membrane and stereocilia of auditory hair cells [5]. This sub-cellular localization was demonstrated using two different methods, immunofluorescence and transfection of organotypic rodent cochlear cultures [5]. Due to its homophilic properties, RIPOR2 has been shown to form ring-like structures near the basal taper of stereocilia [6]. These peculiar arrangement has been proposed to be critical for the shape and length of each individual stereocilium and for proper mechanotransduction

[6]. However, there are additional phenotypic characteristics in the *Ripor2* deficient auditory hair cells that are not totally explained by this pattern of expression. These include the impaired shape and orientation of the hair cell bundle (Fig. 1C, 1D, 2A, 2B) and the mislocalization of the kinocilium (Fig. 2A, B) [6]. For example, Taperin (encoded by the *Tprn* gene) is prominently present at the taper region of stereocilia. However, *Tprn* deficient mice exhibit progressive degeneration of inner hair cell stereocilia with normal hair bundle orientation [18].

Ripor2 has been shown to interact with RhoC as determined by yeast-two-hybrid experiments [6, 8]. Transfection experiments of cochlear explants showed that RhoC co-localized with Ripor2 in stereocilia and regulates Ripor2 oligomerization [6]. Albeit the power of this approach, yeast-two-hybrid possesses some intrinsic limitations including the lack of detecting protein interactions influenced by PTMs [19]. Immunoprecipitation methods do not possess this limitation. Immunoprecipitation has been utilized to unveil the interaction between acetylated Ripor2 with histone deacetylase 6 (HDAC6) and dysferlin in muscular tissue [7]. In this study, we present a previously unrecognized RIPOR2 interacting protein partner: the non- muscular myosin heavy chain 9 (Myh9). *Myh9* deficiency is embryonic lethal in mice [20]. In humans, heterozygous mutations in *MYH9* cause a disorder with a continuous clinical spectrum including hearing loss, for which the term "*MYH9*-related disease" has been suggested [21]However, progressive non-syndromic sensorineural deafness (DFNA17) [9, 22] is also caused by dominant mutations in the *MYH9* gene. A dominant-negative effect has been proposed as mechanism of disease because mutant MYH9 protein dimerizes with the wild type protein to form inclusions [23]. Mammalian cells are equipped with three isoforms of non-muscle myosin II (NMII), termed IIA, IIB and IIC. NM II molecules are comprised of three pairs of proteins: two heavy chains, two regulatory light chains that regulate NM II activity and two essential light chains that stabilize the heavy chain structure [24]. Their heavy chains determine the isoform, which are encoded by three different genes *MYH9*, *MYH10,* and *MYH14*. Little is known about the expression pattern of Myh9 in auditory sensorial epithelium. Previous studies show controversial subcellular localization including stereocilia [14] or along the apical junctional line [25]. Experiments conducted in non-auditory cell lines expressing tagged-MYH9 show that this protein provides coupling between microtubules and the actomyosin system [26]. In the present study, we show that Myh9 is expressed in stereocilia and its abundance is influenced by the presence or absence of Ripor2 (Fig. 4B, C, D). This effect takes place at post-transcriptional level because Myh9 transcripts in *Ripor2* KO cochlea are not reduced (Fig. 4E). Likely, Myh9 stability is enhanced either by direct or indirectly interaction with Ripor2.

Like other isoforms of NMII, the domain structure of NMIIA consists of two globular head domains, a neck domain and a long rod-shaped domain [24]. The head domains contain the binding sites for both ATP and actin, the neck domain acts as a lever arm that amplifies mechanical movement of the head upon hydrolysis of ATP and, the rod domain that effects dimerization of the heavy chains [24]. NMIIA self-associate to form anti-parallel filaments of myosin molecules through the rod domains. NMII folding, assembly and disassembly, actin binding, ATPase and motor activity are tightly regulated by protein PTMs. NMIIA heavy chains are target of phosphorylation by a variety of kinases in the rod region [27].

Phosphorylation affects not only NMIIA filament assembly but also association with actin filaments [27]. In the present study, we show that phosphorylated Myh9 is expressed in the kinocilium of hair cells (Fig. 5A). Its abundance is reduced in the Ripor2 deficient mice (Fig. 5C, D) probably as a result of the downregulation of total Myh9 (Fig. 4C, D). A two-step process for proper cochlear bundle orientation during development has been proposed. The first step consists of the migration of each developing kinocilium towards the lateral edge of the hair cell that occurs between E16 and E18.5 [14, 28], and a subsequent period of refinement in which bundles gradually complete uniform orientation by P10 [28]. Notably, *Ripor2* expression starts between E15.5-E19.5 (Fig. 1B) and persists during postnatal stages in cochlea (Fig. 4A, F). This expression time window coincides with both the migration of kinocilium and the bundle orientation refinement. Since the kinocilium is a key organelle regulating PCP which is affected as early as E18.5 (Fig. 2A, B) in *Ripor2* deficient mice, it is tempting to hypothesize that there is a possible connection between deficiency of Ripor2, downregulation of Myh9/phosphorylated Myh9 and impairment of the kinocilium migration. The downregulation of Myh9 might also affect subsequent bundle orientation refinement. For example, knocking out different ciliary genes generates a spectrum of phenotypic findings ranging from mild cochlear disruptions (e.g. *Gmap210, Ift27, Itt25*) to severe PCP defects (*Ift88* and *Kif3a*) including misplaced stereociliary bundles and shortened cochlear ducts [12]. Such different phenotypes are due to the involvement of ciliary proteins in different cellular processes including, the regulation of the expression of the core PCP transmembrane protein Vangl2 (*Bbs8 or Ift20* mutants), the possession of additional functions beyond the cilia and basal body (e.g. *Ift20* participates in vesicular trafficking from Golgi to the base of the cilium), the dual expression in actin-rich structures and the tubulin-based kinocilium[12], and the regulation of the Wnt signaling pathways (Bbs8) [12]. Similary to other ciliary proteins, we propose that downregulation of Myh9 likely generates the PCP defects on *Ripor2* deficient mice because: Myh9 regulates actomyosin-microtubule crosstalk [26], Ser1943-phosphorylated-Myh9 is highly expressed in the tubulin-based kinocilium (Fig. 5A), and Myh9 localizes in adjacent structures: the kinocilium and the actin reach stereocilia (Fig. 4A and 5A).

Primary cilia develop by the extension of microtubules from one of diplosomal centrioles in various mammal cell types [29]. The rate of primary cilium assembly and stabilization of microtubule structures has been associated with acetylation of K40 in α-tubulin. K40 acetylation has shown to increase microtubule flexibility allowing to better resist mechanical stress [30]Unlike most PTMs of tubulin, K40 acetylation occurs on the luminal side of microtubules [29] and it is primarily controlled by the acetyltransferase Atat1 and the histone deacetylase Hdac6 [31]. Hdac6, a member of the class II HDAC family, is unique in being mainly cytoplasmic. *Hdac6* transcripts are found in mouse cochlear and vestibular hair cells [32]. Unfortunately, we could not extend our analysis of protein distribution of Hdac6 because available antibodies did not show a clear localization in cochlear whole mounts (data not shown). Ripor2 appears to physically interact with Hdac6 [7]. This interaction inhibits Hdac6 deacetylase activity promoting differentiation of myogenic cells [7]. HDAC6 overexpression experiments have been associated with an increase in K40 tubulin acetylation, primary cilium disassembly and length shortening [33]. However, inhibition of HDAC6 activity induce K40 tubulin hyper-acetylation but no effect on cilium length or

count [33]. In fact, the *Hdac6* deficient mice are viable and develop normally [34]. Here we show that absence of Ripor2 associates with a reduced abundance of K40 acetylated α-tubulin in cochlear extracts (Fig. 5E, F). However, we did not find any evidence of change in the length of kinocilia in inner and outer hair cells. Probably, Ripor2 inhibitory effect on Hdac6 and the associated levels of acetylated α-tubulin contributes to kinocilium stabilization and microtubule flexibility during hair bundle morphogenesis. Interestingly, MYH9 has recently been revealed as a novel HDAC6 substrate, being the actin-binding ability of MYH9 regulated by its acetylation status [35]. Because NMIIA expresses in stereocilia (Fig. 4A, F) it would be interesting to study its contribution to the stiffness to the stereociliary actin paracrystal core. It is tempting to hypothesize that Ripor2 may also have a role in conferring shape and length of stereocilia through the Ripor2-Hdac6-Myh9-Actin axis and it is not only limited to its localization in the taper of this organelle.

In summary, we propose additional functions of Ripor2 consisting on the regulation of the abundance and/or PTMs of at least two key components of the kinocilium of auditory hair cells: Myh9-phospho-S1943 and K40 acetylated α-tubulin. Although the kinocilium of inner ear hair cells is not directly involved in auditory perception, its proper development is crucial for hair bundle polarity. The interaction of Ripor2 with multiple proteins distributed along key compartments and organelles within hair cells as well as its own localization justifies the complexity of the phenotype generated by its absence. Clearly, further studies are required to determine to which extend each individual downstream function of Ripor2 contributes to the hearing process.

Supplementary Material

Refer to Web version on PubMed Central for supplementary material.

ACKNOWLEDGEMENTS

This study was supported by NIH grant R01DC009645 to M.T and by the Hearing Health Foundation's Emerging Research Grants program to O.D-H. The Ripor2$^{tm1(KOMP)Vlcg}$ mouse strain used for this research project was created from ES cell clone 15686A-B6, generated by Regeneron Pharmaceuticals, Inc. and made into live mice by the KOMP Repository (www.komp.org) and the Mouse Biology Program (www.mousebiology.org) at the University of California Davis.

References

1. McGrath J, Roy P, Perrin BJ (2016) Stereocilia morphogenesis and maintenance through regulation of actin stability. Seminars in cell & developmental biology. DOI 10.1016/j.semcdb.2016.08.017
2. Axelrod JD (2008) Basal bodies, kinocilia and planar cell polarity. Nature genetics 40: 10–11. DOI 10.1038/ng0108-10 [PubMed: 18163128]
3. Shin JB, Krey JF, Hassan A, Metlagel Z, Tauscher AN, Pagana JM, Sherman NE, Jeffery ED, Spinelli KJ, Zhao H, Wilmarth PA, Choi D, David LL, Auer M, Barr-Gillespie PG (2013) Molecular architecture of the chick vestibular hair bundle. Nature neuroscience 16: 365–374. DOI 10.1038/nn.3312 [PubMed: 23334578]
4. Wu Z, Muller U (2016) Molecular Identity of the Mechanotransduction Channel in Hair Cells: Not Quiet There Yet. The Journal of neuroscience : the official journal of the Society for Neuroscience 36: 10927–10934. DOI 10.1523/JNEUROSCI.1149-16.2016 [PubMed: 27798175]
5. Diaz-Horta O, Subasioglu-Uzak A, Grati M, DeSmidt A, Foster J,, 2nd, Cao L, Bademci G, Tokgoz-Yilmaz S, Duman D, Cengiz FB, Abad C, Mittal R, Blanton S, Liu XZ, Farooq A, Walz K, Lu Z,

Tekin M (2014) FAM65B is a membrane-associated protein of hair cell stereocilia required for hearing. Proceedings of the National Academy of Sciences of the United States of America 111: 9864–9868. DOI 10.1073/pnas.1401950111 [PubMed: 24958875]

6. Zhao B, Wu Z, Muller U (2016) Murine Fam65b forms ring-like structures at the base of stereocilia critical for mechanosensory hair cell function. eLife 5 DOI 10.7554/eLife.14222
7. Balasubramanian A, Kawahara G, Gupta VA, Rozkalne A, Beauvais A, Kunkel LM, Gussoni E (2014) Fam65b is important for formation of the HDAC6-dysferlin protein complex during myogenic cell differentiation. FASEB journal : official publication of the Federation of American Societies for Experimental Biology 28: 2955–2969. DOI 10.1096/fj.13-246470 [PubMed: 24687993]
8. Rolland T, Tasan M, Charloteaux B, Pevzner SJ, Zhong Q, Sahni N, Yi S, Lemmens I, Fontanillo C, Mosca R, Kamburov A, Ghiassian SD, Yang X, Ghamsari L, Balcha D, Begg BE, Braun P, Brehme M, Broly MP, Carvunis AR, Convery-Zupan D, Corominas R, Coulombe-Huntington J, Dann E, Dreze M, Dricot A, Fan C, Franzosa E, Gebreab F, Gutierrez BJ, Hardy MF, Jin M, Kang S, Kiros R, Lin GN, Luck K, MacWilliams A, Menche J, Murray RR, Palagi A, Poulin MM, Rambout X, Rasla J, Reichert P, Romero V, Ruyssinck E, Sahalie JM, Scholz A, Shah AA, Sharma A, Shen Y, Spirohn K, Tam S, Tejeda AO, Trigg SA, Twizere JC, Vega K, Walsh J, Cusick ME, Xia Y, Barabasi AL, Iakoucheva LM, Aloy P, De Las Rivas J, Tavernier J, Calderwood MA, Hill DE, Hao T, Roth FP, Vidal M (2014) A proteome-scale map of the human interactome network. Cell 159: 1212–1226. DOI 10.1016/j.cell.2014.10.050 [PubMed: 25416956]
9. Hildebrand MS, de Silva MG, Gardner RJ, Rose E, de Graaf CA, Bahlo M, Dahl HH (2006) Cochlear implants for DFNA17 deafness. The Laryngoscope 116: 2211–2215. DOI 10.1097/01.mlg.0000242089.72880.f8 [PubMed: 17146397]
10. Valenzuela DM, Murphy AJ, Frendewey D, Gale NW, Economides AN, Auerbach W, Poueymirou WT, Adams NC, Rojas J, Yasenchak J, Chernomorsky R, Boucher M, Elsasser AL, Esau L, Zheng J, Griffiths JA, Wang X, Su H, Xue Y, Dominguez MG, Noguera I, Torres R, Macdonald LE, Stewart AF, DeChiara TM, Yancopoulos GD (2003) High-throughput engineering of the mouse genome coupled with high-resolution expression analysis. Nature biotechnology 21: 652–659. DOI 10.1038/nbt822
11. Yin H, Copley CO, Goodrich LV, Deans MR (2012) Comparison of phenotypes between different vangl2 mutants demonstrates dominant effects of the Looptail mutation during hair cell development. PloS one 7: e31988 DOI 10.1371/journal.pone.0031988 [PubMed: 22363783]
12. May-Simera HL, Petralia RS, Montcouquiol M, Wang YX, Szarama KB, Liu Y, Lin W, Deans MR, Pazour GJ, Kelley MW (2015) Ciliary proteins Bbs8 and Ift20 promote planar cell polarity in the cochlea. Development 142: 555–566. DOI 10.1242/dev.113696 [PubMed: 25605782]
13. Kelly M, Chen P (2007) Shaping the mammalian auditory sensory organ by the planar cell polarity pathway. The International journal of developmental biology 51: 535–547. DOI 10.1387/ijdb.072344mk [PubMed: 17891715]
14. Lim DJ, Anniko M (1985) Developmental morphology of the mouse inner ear. A scanning electron microscopic observation. Acta otolaryngologica Supplementum 422: 1–69
15. Westermarck J, Ivaska J, Corthals GL (2013) Identification of protein interactions involved in cellular signaling. Molecular & cellular proteomics : MCP 12: 1752–1763. DOI 10.1074/mcp.R113.027771 [PubMed: 23481661]
16. Pecci A, Ma X, Savoia A, Adelstein RS (2018) MYH9: Structure, functions and role of non-muscle myosin IIA in human disease. Gene. DOI 10.1016/j.gene.2018.04.048
17. Rai V, Thomas DG, Beach JR, Egelhoff TT (2017) Myosin IIA Heavy Chain Phosphorylation Mediates Adhesion Maturation and Protrusion in Three Dimensions. The Journal of biological chemistry 292: 3099–3111. DOI 10.1074/jbc.M116.733402 [PubMed: 28053086]
18. Jones C, Roper VC, Foucher I, Qian D, Banizs B, Petit C, Yoder BK, Chen P (2008) Ciliary proteins link basal body polarization to planar cell polarity regulation. Nature genetics 40: 69–77. DOI 10.1038/ng.2007.54 [PubMed: 18066062]
19. Bruckner A, Polge C, Lentze N, Auerbach D, Schlattner U (2009) Yeast two-hybrid, a powerful tool for systems biology. International journal of molecular sciences 10: 2763–2788. DOI 10.3390/ijms10062763 [PubMed: 19582228]

20. Matsushita T, Hayashi H, Kunishima S, Hayashi M, Ikejiri M, Takeshita K, Yuzawa Y, Adachi T, Hirashima K, Sone M, Yamamoto K, Takagi A, Katsumi A, Kawai K, Nezu T, Takahashi M, Nakashima T, Naoe T, Kojima T, Saito H (2004) Targeted disruption of mouse ortholog of the human MYH9 responsible for macrothrombocytopenia with different organ involvement: hematological, nephrological, and otological studies of heterozygous KO mice. Biochemical and biophysical research communications 325: 1163–1171. DOI 10.1016/j.bbrc.2004.10.147 [PubMed: 15555549]
21. Seri M, Pecci A, Di Bari F, Cusano R, Savino M, Panza E, Nigro A, Noris P, Gangarossa S, Rocca B, Gresele P, Bizzaro N, Malatesta P, Koivisto PA, Longo I, Musso R, Pecoraro C, Iolascon A, Magrini U, Rodriguez Soriano J, Renieri A, Ghiggeri GM, Ravazzolo R, Balduini CL, Savoia A (2003) MYH9-related disease: May-Hegglin anomaly, Sebastian syndrome, Fechtner syndrome, and Epstein syndrome are not distinct entities but represent a variable expression of a single illness. Medicine 82: 203–215. DOI 10.1097/01.md.0000076006.64510.5c [PubMed: 12792306]
22. Lalwani AK, Goldstein JA, Kelley MJ, Luxford W, Castelein CM, Mhatre AN (2000) Human nonsyndromic hereditary deafness DFNA17 is due to a mutation in nonmuscle myosin MYH9. American journal of human genetics 67: 1121–1128. DOI 10.1016/S0002-9297(07)62942-5 [PubMed: 11023810]
23. Kunishima S, Matsushita T, Kojima T, Sako M, Kimura F, Jo EK, Inoue C, Kamiya T, Saito H (2003) Immunofluorescence analysis of neutrophil nonmuscle myosin heavy chain-A in MYH9 disorders: association of subcellular localization with MYH9 mutations. Laboratory investigation; a journal of technical methods and pathology 83: 115–122 [PubMed: 12533692]
24. Vicente-Manzanares M, Ma X, Adelstein RS, Horwitz AR (2009) Non-muscle myosin II takes centre stage in cell adhesion and migration. Nature reviews Molecular cell biology 10: 778–790. DOI 10.1038/nrm2786 [PubMed: 19851336]
25. Ebrahim S, Fujita T, Millis BA, Kozin E, Ma X, Kawamoto S, Baird MA, Davidson M, Yonemura S, Hisa Y, Conti MA, Adelstein RS, Sakaguchi H, Kachar B (2013) NMII forms a contractile transcellular sarcomeric network to regulate apical cell junctions and tissue geometry. Current biology : CB 23: 731–736. DOI 10.1016/j.cub.2013.03.039 [PubMed: 23562268]
26. Even-Ram S, Doyle AD, Conti MA, Matsumoto K, Adelstein RS, Yamada KM (2007) Myosin IIA regulates cell motility and actomyosinmicrotubule crosstalk. Nature cell biology 9: 299–309. DOI 10.1038/ncb1540 [PubMed: 17310241]
27. Betapudi V (2014) Life without double-headed non-muscle myosin II motor proteins. Frontiers in chemistry 2: 45 DOI 10.3389/fchem.2014.00045 [PubMed: 25072053]
28. Dabdoub A, Donohue MJ, Brennan A, Wolf V, Montcouquiol M, Sassoon DA, Hseih JC, Rubin JS, Salinas PC, Kelley MW (2003) Wnt signaling mediates reorientation of outer hair cell stereociliary bundles in the mammalian cochlea. Development 130: 2375–2384 [PubMed: 12702652]
29. Nakakura T, Asano-Hoshino A, Suzuki T, Arisawa K, Tanaka H, Sekino Y, Kiuchi Y, Kawai K, Hagiwara H (2015) The elongation of primary cilia via the acetylation of alpha-tubulin by the treatment with lithium chloride in human fibroblast KD cells. Medical molecular morphology 48: 44–53. DOI 10.1007/s00795-014-0076-x [PubMed: 24760594]
30. Xu Z, Schaedel L, Portran D, Aguilar A, Gaillard J, Marinkovich MP, Thery M, Nachury MV (2017) Microtubules acquire resistance from mechanical breakage through intralumenal acetylation. Science 356: 328–332. DOI 10.1126/science.aai8764 [PubMed: 28428427]
31. Rao Y, Hao R, Wang B, Yao TP (2014) A Mec17-Myosin II Effector Axis Coordinates Microtubule Acetylation and Actin Dynamics to Control Primary Cilium Biogenesis. PloS one 9: e114087 DOI 10.1371/journal.pone.0114087 [PubMed: 25494100]
32. Shen J, Scheffer DI, Kwan KY, Corey DP (2015) SHIELD: an integrative gene expression database for inner ear research. Database : the journal of biological databases and curation 2015: bav071. DOI 10.1093/database/bav071
33. Ran J, Yang Y, Li D, Liu M, Zhou J (2015) Deacetylation of alphatubulin and cortactin is required for HDAC6 to trigger ciliary disassembly. Scientific reports 5: 12917 DOI 10.1038/srep12917 [PubMed: 26246421]
34. Zhang Y, Kwon S, Yamaguchi T, Cubizolles F, Rousseaux S, Kneissel M, Cao C, Li N, Cheng HL, Chua K, Lombard D, Mizeracki A, Matthias G, Alt FW, Khochbin S, Matthias P (2008) Mice lacking histone deacetylase 6 have hyperacetylated tubulin but are viable and develop normally.

Molecular and cellular biology 28: 1688–1701. DOI 10.1128/MCB.01154-06 [PubMed: 18180281]

35. Zhang L, Liu S, Liu N, Zhang Y, Liu M, Li D, Seto E, Yao TP, Shui W, Zhou J (2015) Proteomic identification and functional characterization of MYH9, Hsc70, and DNAJA1 as novel substrates of HDAC6 deacetylase activity. Protein & cell 6: 42–54. DOI 10.1007/s13238-014-0102-8 [PubMed: 25311840]
36. Toyama EQ, Herzig S, Courchet J, Lewis TL,, Jr., Loson OC, Hellberg K, Young NP, Chen H, Polleux F, Chan DC, Shaw RJ (2016) Metabolism. AMP-activated protein kinase mediates mitochondrial fission in response to energy stress. Science 351: 275–281. DOI 10.1126/science.aab4138 [PubMed: 26816379]

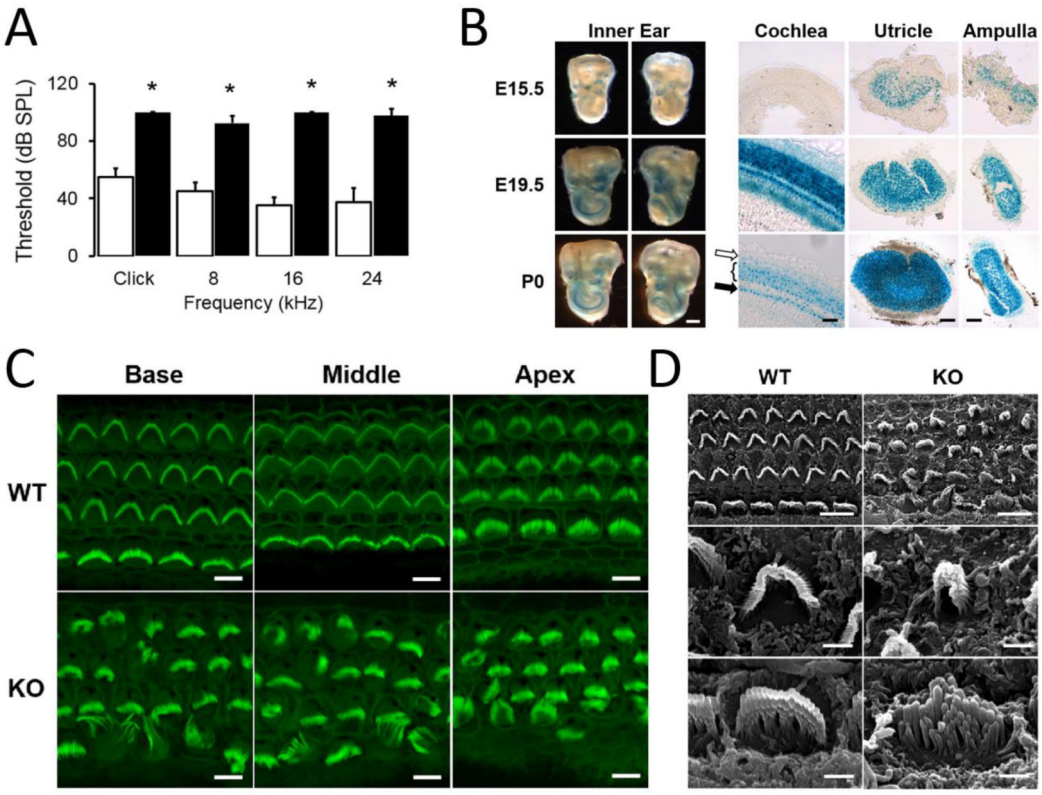

Figure 1.

Analysis of hearing function, gene expression and hair cell morphology of *Ripor2*deficient mice *(A)* Increased ABR thresholds in 8–10-week-old *Ripor2* KO mice show (n=4, black columns) in comparison with wild type mice (n=4, white columns), (* p<0.0001, two-way ANOVA and t-test pairwise comparisons). Values are represented as average ± SD. *(B)* X-gal staining of whole inner ear, cochlea, utricle and ampulla from E15.5, E19.5, and P0 *Ripor2*$^{+/-}$ heterozygous mice. At P0, LacZ is expressed in inner hair cells (black arrow), outer hair cells (left brace) and Hensen's cells (white arrow). Scale bars: Inner ear (200 μm), Cochlea, Utricle and Ampula (40 μm). *(C)* Representative single plane confocal images of apical stereocilia in cochlear whole mounts from wild type and *Ripor2* KO mice at P4. Alexa Fluor 488 Phalloidin (green) was used for F-actin staining, scale bar: 8 μm. *(D)* Analysis of hair cells and stereocilia by SEM. Upper panels are low magnification images showing morphology of hair cells, scale bar: 5 μm. Middle and lower panels are high magnification images of outer and inner hair cells, respectively, showing the stereociliary bundle morphology, scale bars: 5 μm.

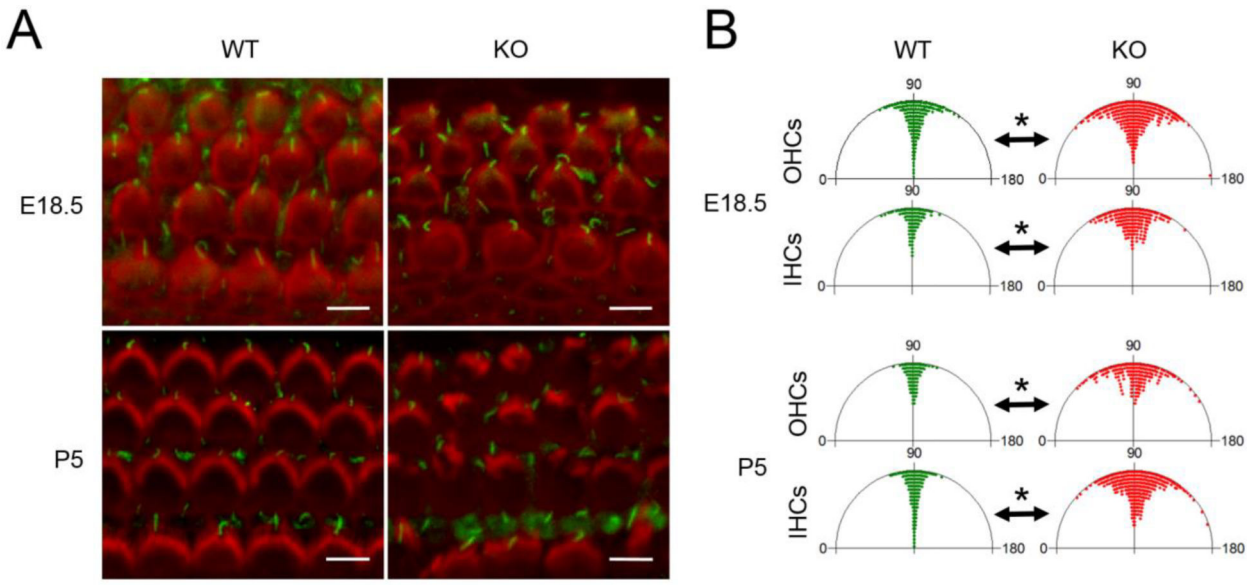

Figure 2.

Planar cell polarity in the developing cochlea of Ripor2 deficient mice. *(A)* Representative single plane confocal images showing the kinocilium position and the bundle orientation of outer and inner hair cells in cochleae from wild type and Ripor2 deficient mice at E18.5 and P5. Kinocilia and the stereociliary bundles were stained with an acetylated-α-tubulin antibody (green signals) and phalloidin (red signals), respectively. *(B)* Bundle orientation plots generated using Oriana 4 circular graphing software (Kovach Computing Services). Each dot represent individual stereociliary bundle orientation angles with 90º indicating the normal angle formed between the longitudinal axis and mediolateral axis. Measurements (n>100 per each plot) were taken in all three different portions of the length of the cochlea (base, middle and apex) from *Ripor2* KO (red) and wild type (green) mice at E18.5 and P5. Statistical significance was analyzed by chi-square.*$p<1\times10^{-10}$. Scale bar: 5 μm.

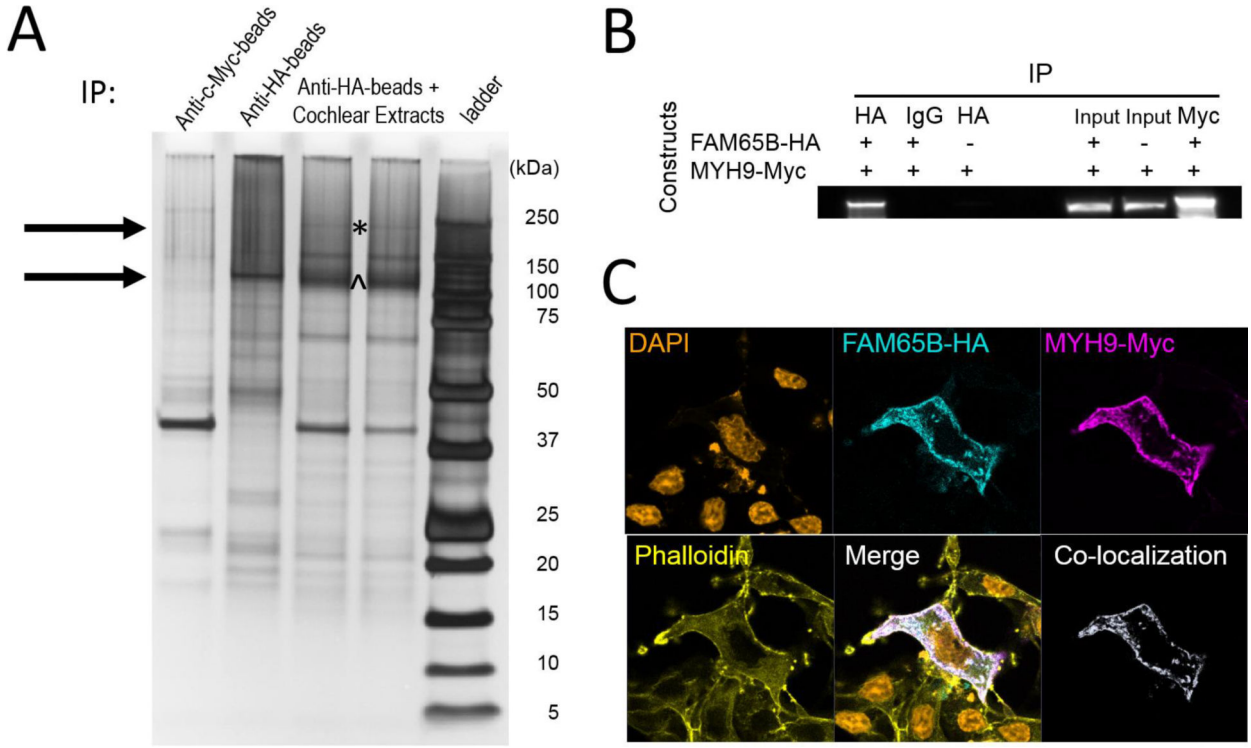

Figure 3.

Interaction of RIPOR2 and MYH9 *(A) Silver stain of IP extracts separated in a SDS- PAGE gel.* HEK293 cells were transfected with a RIPOR2-HA coding plasmid. Lane 1 shows proteins precipitated with anti-c-Myc antibody coupled beads as control; lane 2, proteins precipitated with anti-HA antibody coupled beads; lane 3 and 4, proteins from transfected HEK293 cells combined with wild type mouse dissected cochlear extracts and precipitated with anti-HA antibody coupled beads. This two lanes are a duplication in order to gather sufficient material for MS analysis after band excision. The molecular size of the bands from a protein standard ladder (lane 5) is indicated in kilodaltons (kDa). After MS analysis, the bands indicated with an asterisk correspond to Myh9 of approximately 226 kDa molecular weight. The bands indicated with a ^ corresponds to the RIPOR2-HA tagged protein. *(B) Confirmation of RIPOR2 and MYH9 co-immunoprecipitation by western blotting.* HEK293 cells were transfected with the constructs indicated. Immunoprecipitations were carried out with anti-HA or anti-Myc antibodies, followed by western blotting using and anti-Myc antibody. Immunoprecipitation negative control experiments included a pulldown with non-specific mouse IgGs and an anti-HA pulldown with protein extracts lacking HA-tagged RIPOR2. Input protein signals were also tested as indicated. *(C) Co-localization of RIPOR2 and MYH9 evaluated by immunofluorescence.* COS-7 cells were transfected with RIPOR2-HA and MYH9-Myc expression vectors. Nuclei and f-actin were counterstained using DAPI and phalloidin, respectively. The B&W image results from a co-localization highlighter plugin (ImageJ)(12). The calculated average co-localization percent is 84%.

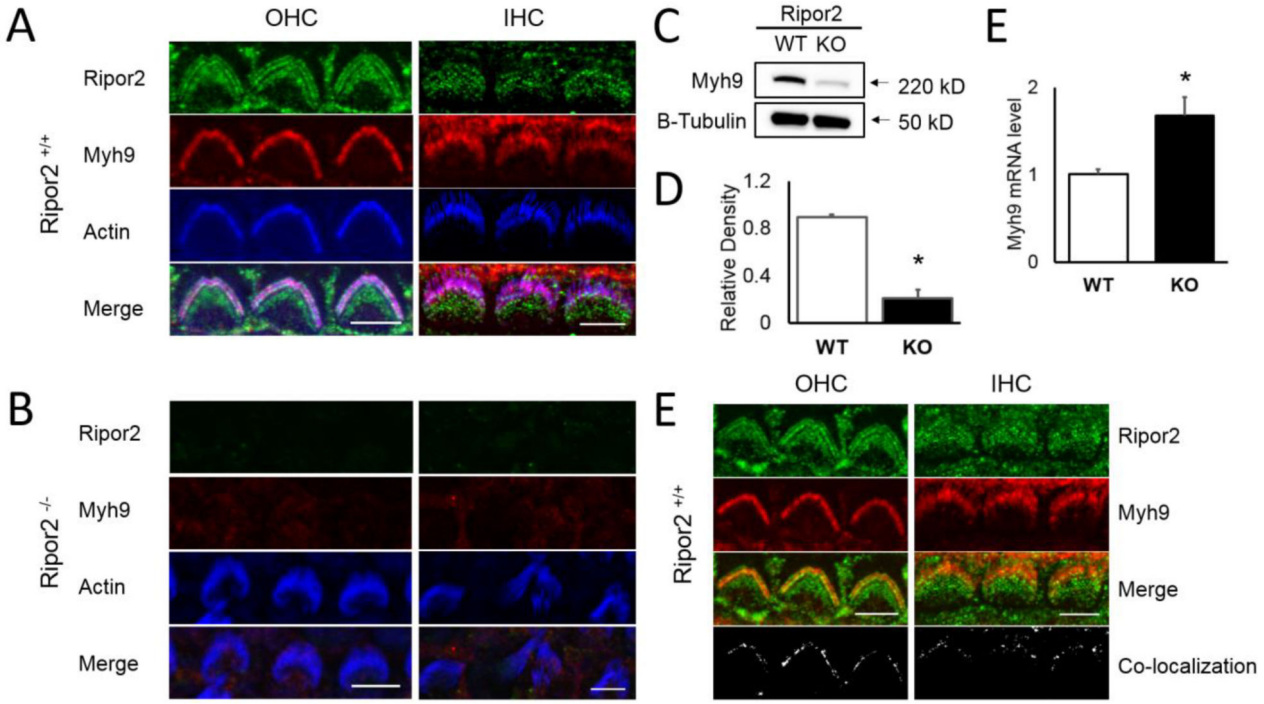

Figure 4.

Localization and abundance of Myh9 in cochlea of wild type and *Ripor2* deficient mouse. (*A and B*) Representative single plane confocal images showing expression of Ripor2 and Myh9 to the stereocilia of outer and inner hair cells in wild type *(A)* and *Ripor2* deficient mice *(B)*. Sample preparation was performed in parallel for both specimens. The conditions for the capture of images and the laser intensities were the same for both samples. Whole mount cochleae from P4 mice were immunostained using an anti-Ripor2 rabbit polyclonal (HPA031245, Sigma) and an anti-Myh9 mouse monoclonal antibody (H00004627-M01, Abnova). Alexa Fluor 647 Phalloidin (Blue) was utilized for F-actin staining to visualize the stereociliary bundle. Scale bar: 5 μm. *(C)* Amount of Myh9 in wild type and *Ripor2* KO mouse cochleae. Cell lysates from P4 mouse cochleae were analyzed by western blotting using a primary mouse monoclonal antibody (H00004627-M01, Abnova) to detect total Myh9. The loading control β-tubulin was detected using a rabbit polyclonal antibody (ab15708, EMD Millipore). *(D)* Relative density of bands from three western blot independent experiments were measured using Image J. Results are presented as average ± SD, * $p<0.01$, t-test for independent samples. *(E)* Expression levels of *Myh9* amplicons were determined by qPCR using RNA extracted from P4 mouse cochleae, SYBR Select Master Mix (Thermofisher) and primers mMyh9_F and mMyh9_R (Table S1). Values are represented as average ± SD, *$p<0.05$, t-test for independent samples. *(F)* Representative single plane confocal images showing Ripor2 and Myh9 co-localizing to the base of stereocilia in outer and inner hair cells of wild type mice. B&W images result from the co-localization highlighter plugin (ImageJ) [36]. Scale bar: 5 μm.

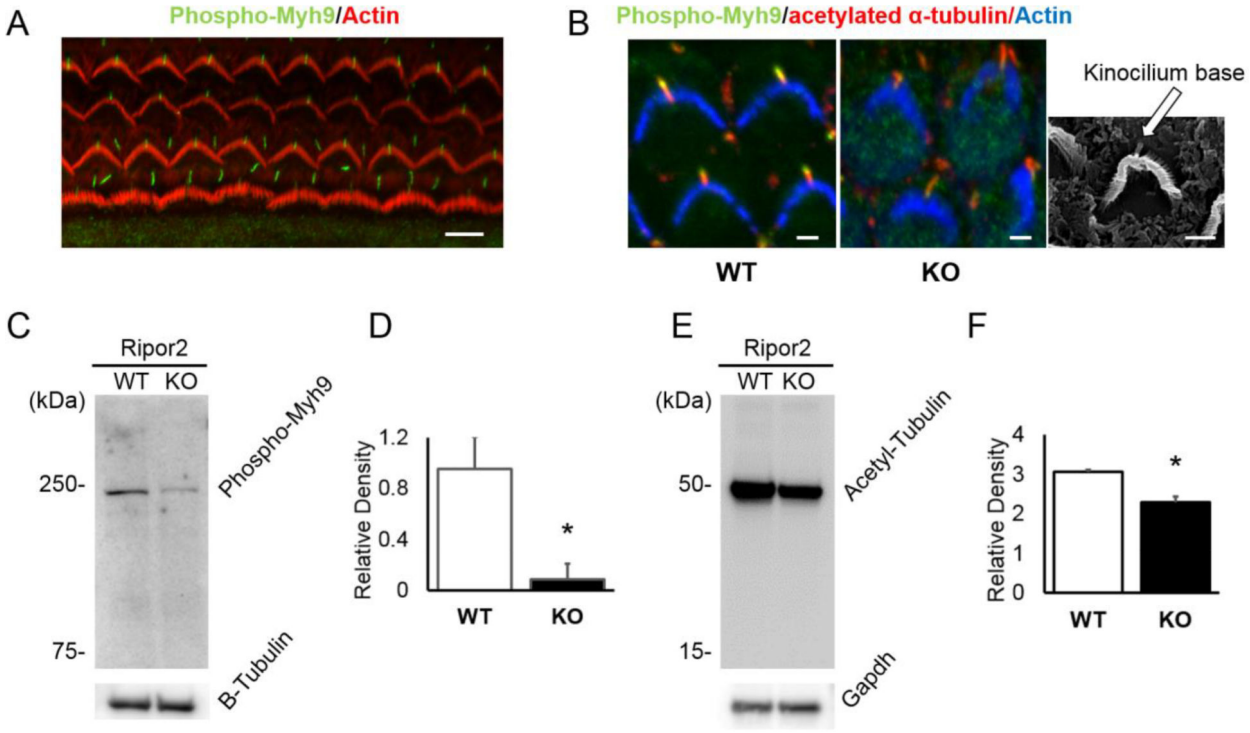

Figure 5.

Abundance and expression of phospho-Myh9 and Acetyl-α-tubulin in cochlea of wild type and *Ripor2* deficient mouse. *(A)* Representative Z-stack merged projections showing that the pattern of expression of phosphorylated-Myh9 is similar to the kinocilium of inner and outer hair cells and the primary cilium of supporting cells. Whole mount cochlea from P4 wild type mice was immunostained using an anti-Myh9-phospho-S1943 rabbit polyclonal antibody (ab2974, EMD Millipore). Scale bar: 8 μm. *(B)* Representative Z-stack merged projections showing expression of phospho-Myh9, alpha-acetyl tubulin, and stereociliary actin in P4 WT and *Ripor2* KO mice. A SEM image is presented to indicate the base to tip orientation of the kinocilium. Scale bars: 2 μm. *(C)* Amount of phospho-Myh9 in wild type and *Ripor2* KO mice. Cell lysates from P4 mouse cochleae were analyzed by western blotting using an anti-Myh9-phospho-S1943 rabbit polyclonal antibody (ab2974, EMD Millipore). The loading control β-tubulin was detected using a rabbit polyclonal antibody (ab15708, EMD Millipore). *(D)* Relative density of bands from three independent experiments were measured using Image J. Results are presented as average ± SD, * $p<0.01$, t-test for independent samples. *(E-F)* Effect of *Ripor2* deficiency on the abundance of acetylated tubulin in mouse cochlea. *(E)* Cell lysates from P4 mouse cochleae were analyzed by western blotting using anti-acetyl-K40-α-tubulin (Lys 40) rabbit monoclonal antibody (D20G3, Cell Signaling Technology). The loading control Gapdh was detected using a mouse monoclonal antibody (sc-47724, Santa Cruz Biotechnology). *(F)* Relative density of bands from three independent experiments were measured using Image J. Results are presented as average ± SD, * $p=0.001$, t-test for independent samples.